Three-dimensional object profiling using highly accurate FMCW optical ranging system

著者	Ula Rini Khamimatul, Noguchi Yusuke, Iiyama Koichi
著者別表示	飯山 宏一
journal or publication title	Journal of Lightwave Technology
volume	37
number	15(8732446)
page range	3826-3833
year	2019-08-01
URL	http://doi.org/10.24517/00059005

doi: 10.1109/JLT.2019.2921353

Creative Commons : 表示 - 非営利 - 改変禁止
http://creativecommons.org/licenses/by-nc-nd/3.0/deed.ja

Three-dimensional object profiling using highly accurate FMCW optical ranging system

Rini Khamimatul Ula, *Member, OSA*, Yusuke Noguchi, and Koichi Iiyama, *Member, IEEE*

***Abstract*—We have developed three-dimensional object profiling system using a highly accurate FMCW optical ranging system. A DFB laser and a VCSEL are used as the laser source and the optical frequency is swept by the injection current modulation with a symmetric triangular wave. The influence of nonlinearity in the optical frequency sweep is canceled by utilizing k-sampling technique. Since the optical frequency sweep range of a VCSEL is larger than that of a DFB laser, high spatial resolution and high ranging accuracy are achieved by using a VCSEL. The spatial resolution evaluated by the full-width at half maximum (FWHM) is 460 μm and the standard deviation of the ranging accuracy is $\sigma = 2.7\,\mu$m when a VCSEL is used as the frequency-swept laser source, and the FWHM is 2.3 mm and $\sigma = 14.8\,\mu$m when a DFB laser is used as the frequency-swept laser source. Accordingly, fine and clear object profiling of a coin and a printed circuit board is achieved by using a VCSEL as the frequency-swept laser source. Finally we speed-up the measurement time by increasing the repetition frequency of the injection current modulation and optimizing timing of the data acquisition, the galvano mirror scan and the FFT analysis by taking account of the transient response of the galvano mirror, and the fastest measurement time of 22.6 sec is achieved for 201×201 points measurement points, which is four times faster than our previous results. We also discuss the effect of moving average filtering and median filtering to improve profiling quality.**

***Index Terms*—FMCW optical ranging system, Object profiling, Optical imaging**

I. Introduction

Frequency-modulated continuous-wave (FMCW) optical ranging system is a high-resolution interferometric ranging system using an optical frequency-swept laser source [1], [2]. Fig. 1(a) shows the configuration of the FMCW optical ranging system. The FMCW optical ranging system is composed of a frequency-swept laser source and a two-beam interferometer, and a target is located in an arm of the interferometer. The reflected light from the target interferes with the reference light reflected from the mirror on a photodetector (PD). The reflected light is delayed with respect to the reference light by $\tau = 2nL/c$, where L is the differential distance between the reflected and the reference lights, n is the refractive index, and c is the light speed in vacuum. When the optical frequency of the laser source is swept with a symmetric triangular waveform

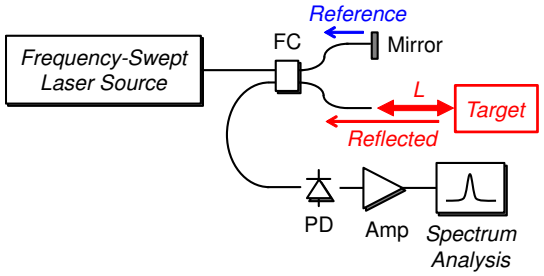

(a) Configuration (PD: Photodetector, FC: Fiber coupler).

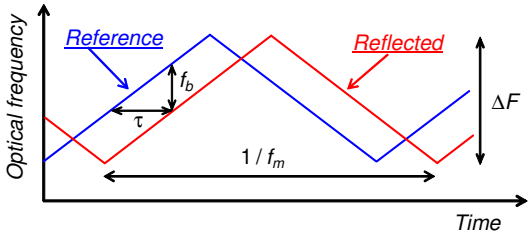

(b) Waveform of optical frequency change.

Fig. 1. Configuration of the FMCW optical ranging system and the waveform of the optical frequency change of the reference and the reflected lights.

as is shown in Fig. 1(b), the interference signal has a beat frequency f_b given as;

$$f_b = 2f_m \Delta F \times \tau = \frac{4nf_m \Delta F}{c} L \tag{1}$$

where f_m and ΔF are the repetition frequency of the optical frequency sweep and the optical frequency sweep range, respectively. The beat frequency f_b is proportional to the distance L, and then the distance L can be measured by the Fourier analysis of the interference signal. The interference signal in the increasing or decreasing section of the modulation signal shown in Fig. 1(b) is usually measured to avoid phase discontinuity in the interference signal at the turning points of the optical frequency sweep, and then the beat spectrum is obtained by the FFT. This means that the time domain width for the FFT is $1/(2f_m)$ and the beat spectrum is described by the sinc function, and then the spatial resolution δL defined by the Rayleigh resolution is given as;

$$\delta L = \frac{c}{2n\Delta F}. \tag{2}$$

If there are multiple reflection points in the target, multiple peaks are observed in the beat spectrum and the locations of the multiple reflection points can be measured from the beat frequencies of the multiple peaks. Distributed sensing is then possible by spectrum analysis of the interference

Manuscript received mmmm dd, 2018; revised mmmm dd, 2019. This work was supported by JSPS KAKENHI Grant Number JP24560517, JP17K06457.

The authors are with Division of Electrical Engineering and Computer Science, Graduate School of Natural Science and Technology, Kanazawa University, Kakuma-machi, Kanazawa 920-1192, Japan (e-mail: iiyama@se.kanazawa-u.ac.jp)

R. K. Ula is also with the Research Center for Physics, Indonesia Institute of Sciences, Indonesia.

signal. Actually the FMCW optical ranging system has been actively studied as the FMCW reflectometry, also known as the coherent optical frequency domain reflectometry (OFDR), to characterize and diagnose optical fibers and optical waveguides [3]–[12]. In optical reflectometry application, high spatial resolution is desired to distinguish adjacent fault locations.

The other applications of the FMCW optical ranging system are optical coherence tomography (OCT) and object profiling [13]–[17]. For imaging human eye and fingertip, high spatial resolution is the most important performance because of their small size, and the spatial resolution of about 10 μm is realized for the measurement range of about 1 cm. For object profiling, the measurement range should be longer than the case of imaging human eye and fingertip. The spatial resolution of 15 μm at the distance of about 70 cm are achieved by using a MEMS-VCSEL (micro electro mechanical systems vertical cavity surface emitting laser) as the frequency-swept laser source [13]. We have demonstrated tentative experimental results of object profiling using a DFB laser and a VCSEL as the frequency-swept laser source [15], [16]. The optical frequency of the DFB laser and the VCSEL are swept by the injection current modulation, and the VCSEL is found to be a suitable laser source for accurate object profiling because of the large optical frequency sweep range. In the report [16], the repetition frequency of the optical frequency sweep $f_m = 500$ Hz and the resultant measurement time for 201×201 measurement points was about 84 sec.

Here we describe performance of object profiling using the FMCW ranging system when a DFB laser and a VCSEL are used as the frequency-swept laser source. We also describe speed-up of object profiling by increasing the repetition frequency of the optical frequency sweep and optimizing timing of the data acquisition, the galvano mirror scan and the FFT analysis by taking account of transient response of the galvano mirror. The final measurement time is four times faster than our previous report [16]. We also discuss the effect of moving average filtering and median filtering to improve profiling quality.

II. System Configuration

Figure 2 shows the experimental setup of the FMCW optical ranging system. A laser diode emitting at 1310 nm is used as a light source and the optical frequency is swept by modulating the injection current with a symmetric triangular signal with the repetition frequency $f_m = 1$ kHz. Two types of laser diodes are used as the laser source; a DFB laser (Furukawa, FOL13F1MWS-A4-SA7) and a sngle-mode VCSEL (RayCan, RC22xxx1-T). The threshold current, the maximum current, the bias current and the modulation current amplitude of the DFB laser and the VCSEL are tabulated in Table I.

The laser light is launched from the circulator (Cir) onto the target to be profiled, and the reflected light from the target interferes with the reference light passed through the fiber couplers FC2 and FC3. The laser light is focus on the target by the lens with the focal length of 20 cm. The beam size at the focal point of the lens is not measured, however is deduced to be a few tens μm from the profiling results as

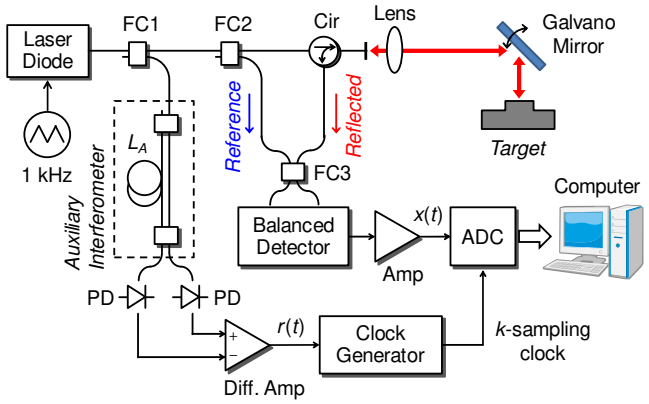

Fig. 2. Experimental setup of the FMCW optical ranging system for object profiling (FC1, FC2, FC3: Fiber couplers, Cir: Circulator, PD: Photodiode).

TABLE I
THE BIAS AND THE MODULATION CONDITIONS OF THE DFB LASER AND THE VCSEL.

Parameter	Notation	DFB	VCSEL
Threshold current	I_{th}	20 mA	1.2 mA
Maximum current	I_{max}	150 mA	15 mA
Bias current	I_{DC}	90 mA	8 mA
Modulation amplitude	ΔI	100 $mA_{p\text{-}p}$	12 $mA_{p\text{-}p}$
Optical frequency sweep range	ΔF	136 GHz	710 GHz
Theoretical spatial resolution	δL	1.10 mm	211 μm
Theoretical FWHM	δL_{FWHM}	2.20 mm	422 μm

shown later. Since the repetition frequency of the injection current modulation is as slow as 1 kHz, the optical frequency of the DFB laser and the VCSEL is modulated by thermal effect in the laser cavity. The optical frequency change of the DFB laser and the VCSEL lags behind the injection current change due to slow temperature change in the laser cavity, and the optical frequency is nonlinearly swept. As a result, the spatial resolution and the ranging accuracy are seriously degraded.

To eliminate the influence of nonlinearity in the optical frequency sweep, we utilized k-sampling technique. The k-sampling clock is generated from the interference signal of the auxiliary interferometer, $r(t)$ in Fig. 2, and the sensing interference signal, $x(t)$ in Fig. 2, is sampled with the k-sampling clock. The beat spectrum of the sampled sensing interference signal is analyzed by the FFT. The target is profiled by scanning the laser light over the target by using a two-dimensional galvano mirror (Thorlabs, GVS002).

In the k-sampling technique, the Sampling theorem should be satisfied between the sensing interference signal $x(t)$ and the auxiliary interference signal $r(t)$. The measurement range L_{max} is given as [12]

$$L_{max} = \frac{1}{4} n L_A \tag{3}$$

by considering that the sensing interferometer is Michelson-type and the auxiliary interferometer is Mach-Zehnder-type, where n and L_A are the refractive index and the length of the fiber delay line in the auxiliary interferometer, respectively. When the beat frequency appears at the data point D in the

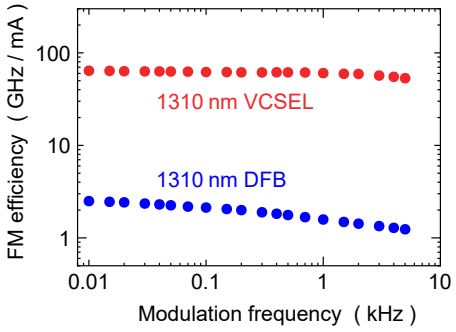

Fig. 3. Measured frequency modulation (FM) efficiency of the 1310 nm VCSEL and the 1310 nm DFB laser.

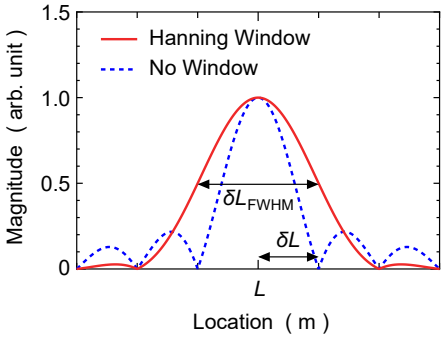

Fig. 4. Schematic beat spectrum and definition of the spatial resolution.

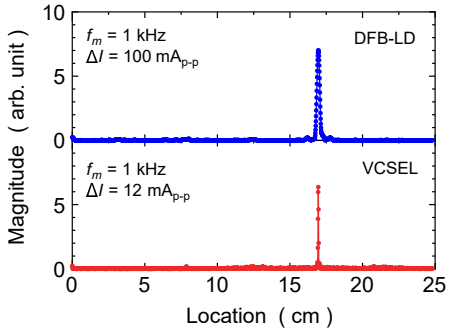

(a) Whole beat spectrum.

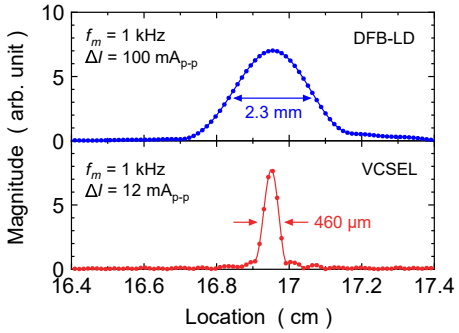

(b) Enlarged beat spectrum round the peak.

Fig. 5. Measured reflection profile for a mirror located around 17 cm.

beat spectrum, the distance L is given as;

$$L = \frac{D}{N/2} L_{max} = \frac{nL_A}{2N} D \tag{4}$$

where N is the number of data used in the FFT analysis. Since the beat spectrum is discrete, the exact distance cannot be obtained from the peak position of the beat spectrum. The exact distance is evaluated by parabolic fitting around the peak in the beat spectrum. The value of nL_A is adjusted to be $nL_A = 1$ m, and the resultant measurement range is $L_{max} = 25$ cm. In the measurement, the interference signal in the increasing section of the modulating triangular signal is acquired. The number of acquired data is 450 points when the DFB laser is used as the frequency-swept laser source and is 2350 points when the VCSEL is used as the frequency-swept laser source. The difference of the number of acquired data is attributed to the difference of the optical frequency sweep range ΔF. In the FFT analysis, zero values are added to the acquired data after multiplying the Hanning window function to the acquired data (zero padding method), and the beat spectrum is calculated for totally 4096 points to obtain dense FFT spectrum without degrading the spatial resolution.

Figure 3 shows the measured frequency modulation (FM) efficiency of the 1310 nm VCSEL and the 1310 nm DFB laser. The FM efficiency at 1 kHz is 1.6 GHz/mA for the DFB laser and 60 GHz/mA for the VCSEL. The FM efficiency of the VCSEL is 38 times larger than that of the DFB laser. As shown in Table I, the modulation current amplitude is 100 $mA_{p\text{-}p}$ for the DFB laser and is 12 $mA_{p\text{-}p}$ for the VCSEL, and the resultant optical frequency sweep range ΔF is about 135 GHz for the DFB laser and 710 GHz for the VCSEL. Therefore high spatial resolution is expected by using the VCSEL as the frequency swept laser source. The optical frequency sweep range ΔF shown in Table I is slightly smaller than the value calculated by the product of the FM efficiency and the modulation current amplitude ΔI because the interference signal around the turning points of the modulation waveform is not used for the FFT analysis.

In Table I, we defined the theoretical full-width at half-maximum (FWHM) as a measure of the spatial resolution. Figure 4 shows a schematic beat spectrum without using a window function (dashed line) and with the Hanning window (solid line) in the FFT. The spatial resolution given in eq. (2) is defined as the differential distance between the peak and the first zero point in the $|\mathrm{sinc}|$ function, which is the beat spectrum without using a window function in the FFT. In our experiments, we used the Hanning window in the FFT, and the spatial resolution was estimated from the FWHM of the beat spectrum, which is expressed as δL_{FWHM} in Fig. 4. The theoretical FWHM using the Hanning window is given as;

$$\delta L_{\mathrm{FWHM}} = 2\delta L = \frac{c}{n\Delta F}. \tag{5}$$

III. Spatial Resolution and Ranging Accuracy

Figure 5(a) shows the measured beat spectrum for a mirror located around 17 cm, and Fig. 5(b) is the enlarged beat spectrum. Fine beat spectra are observed around 17 cm, and the beat spectrum when the VCSEL is used is narrower than the beat spectrum when the DFB laser is used. The measured FWHM is 2.3 mm when the DFB laser is used and is 460 μm when the VCSEL is used, which are almost the same with the theoretical FWHM shown in Table 1. As expected, high spatial

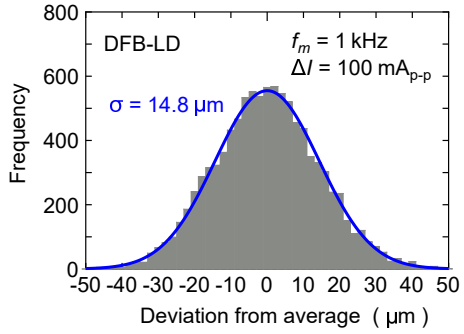

(a) When the DFB laser is used.

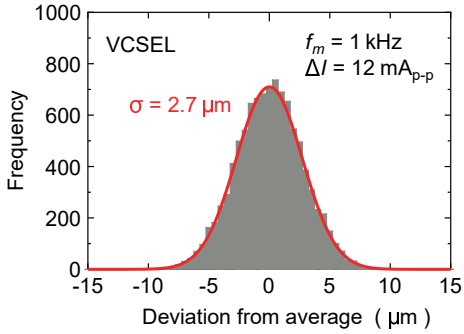

(b) When the VCSEL is used.

Fig. 6. Histogram of the measured distance error for 10000-times measurements at the distance of 17 cm.

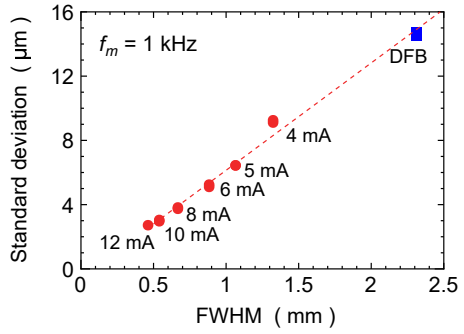

Fig. 7. Relationship between the FWHM and the standard deviation.

resolution is achieved by using the VCSEL as the frequency-swept laser source due to wider optical frequency sweep range ΔF.

Figure 6 shows an example of histograms of the measured distance error; (a) is the result when the DFB laser is used, and (b) is the result when the VCSEL is used. A mirror is located at 17 cm, and the distance to the mirror is measured 10000 times. The mirror is put on a measurement table and is not fixed on the measurement table. The horizontal axis is the deviation from the averaged distance, and the vertical axis is the frequency. The solid curves are the normal distribution with the standard deviation $\sigma = 14.8\,\mu$m for (a) and $\sigma = 2.7\,\mu$m for (b). Smaller measurement error is obtained by using the VCSEL as the frequency-swept laser source.

We measured the FWHM of the beat spectrum and the standard deviation with different modulation current amplitude ΔI, and the relation between the FHWM and the standart deviation is shown in Fig. 7. The repetition frequency of the

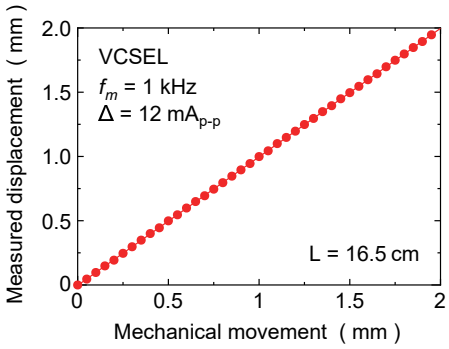

Fig. 8. Measured displacement against the small displacement.

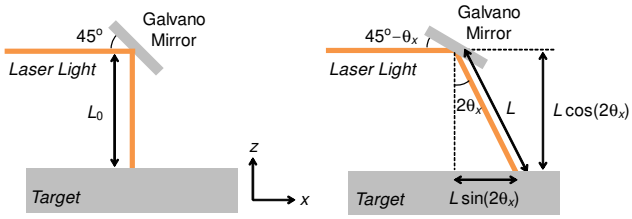

(a) Initial angle. (b) Angle changed by θ_x.

Fig. 9. Schematics of the propagation of the laser light after reflected by a one-dimensional galvano mirror.

injection current modulation $f_m = 1$ kHz. The peak-to-peak current modulation amplitude is shown in the figure, and the result when a DFB laser is used is also shown in the figure. The standard deviation is proportional to the FWHM, and then highly accurate object profiling can be achieved by enhancing the spatial resolution.

Next we measure the beat spectrum when the location of the mirror is slightly changed to confirm whether small distance changes can be accurately measured. Figure 8 shows the measured displacement against the small displacement of a mirror located around 16.5 cm. The displacement is accurately measured and the measured displacement agrees well with the mechanical displacement. From Figs. 6 $\sim$ 8, clear object profiling of small mechanical workpieces is expected.

IV. Object Profiling

Next we measured the profiles of a coin and a printed circuit board by two-dimensionally scanning the laser light by using a two-dimensional galvano mirror as shown in Fig. 2.

Figure 9 shows the schematics of the propagation of the laser light after reflected by a one-dimensional galvano mirror. The initial angle of the galvano mirror is 45° as shown in Fig. 9(a) and the laser light is normally illuminated onto the target, and the distance L_0 is measured by the FMCW optical ranging system. If the angle of the galvano mirror is changed by θ_x with respect to 45° in the x-direction, the illuminating angle is changed by $2\theta_x$ as shown in Fig. 9(b), and the diagonal length to the target L is measured by the FMCW optical ranging system. Then the horizontal distance change x and the height

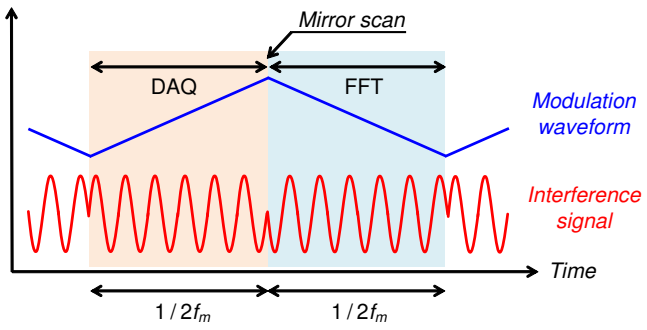

Fig. 10. Timings of the data acquisition (DAQ), the galvano mirror scan, and the FFT analysis.

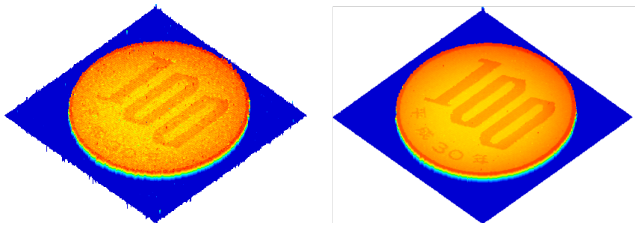

(a) When a DFB laser is used. (b) When a VCSEL is used.

Fig. 11. Three-dimensional profiling result of a Japanese 100YEN coin.

z at the illuminated point are calculated as;

$$\begin{aligned} x &= L\sin(2\theta_x) \\ z &= L\cos(2\theta_x). \end{aligned}$$

A two-dimensional galvano mirror is used in our FMCW optical ranging system. If the angle of the galvano mirror is changed by θ_x and θ_y in the x-direction and the y-direction, respectively, the illuminating angle is change by $2\theta_x$ and $2\theta_y$ in the x-direction and the y-direction, respectively. As a result, the horizontal distance change x and y and the height z at the illuminated point are calculated from the measured diagonal length to the target L as;

$$x = L\sin(2\theta_x) \quad (6)$$
$$y = L\sin(2\theta_y) \quad (7)$$
$$z = L\cos(2\theta_x)\cos(2\theta_y). \quad (8)$$

Figure 10 shows the timing of the data acquisition (DAQ), the galvano mirror scan and the FFT analysis. The optical frequency of the laser source is swept by modulating the injection current with a symmetric triangular signal. The interference signal in the increasing section of the modulation waveform is acquired, and the galvano mirror is scanned to the next position after the data acquisition, and then the acquired data is FFT analyzed. As a result, one distance measurement is completed within the period of $1/f_m$.

Figure 11 shows the measured profile of a Japanese 100YEN coin (a) when the DFB laser is used and (b) when the VCSEL is used. The number of acquired data is (a) 450 points and (b) 2350 points, and the number of the FFT analysis is 4096 points by using the zero padding method. The angle of the galvano mirror is changed from $-2.5\,^\circ$ to $+2.5\,^\circ$ in $0.025\,^\circ$ increment and the corresponding profiled area is

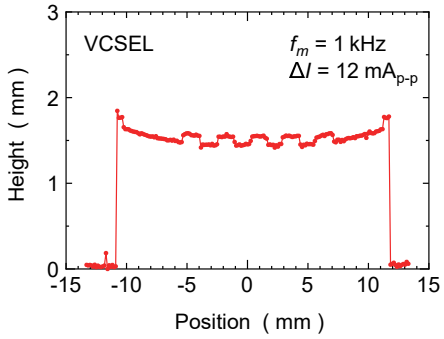

Fig. 12. Two-dimensional profiling result around the center of the Japanese 100YEN coin.

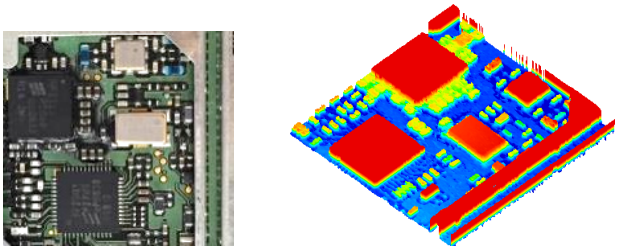

(a) Photograph. (b) Profiled result.

Fig. 13. Photograph and the three-dimensional profiling result of a printed circuit board.

$26.5 \times 26.5\,\mathrm{mm}^2$. The resultant profiled data is 201×201 points, and the measurement time is about 42 sec. It is found that fine and clear profiling is obtained when the VCSEL is used as compared to the result when the DFB laser is used due to the smaller measurement error as shown in Fig. 6. We can successfully image the incuse on the surface of the coin (labels "100" and Japanese traditional era name) by using a VCSEL as the frequency-swept laser source.

Figure 12 shows the two-dimensional profile around the center of the Japanese 100YEN coin when the VCSEL is used. The thickness of the coin is found to be about 1.7 mm at the edge of the coin and about 1.5 mm at the center of the coin, and the surface of the coin is slightly curved. The step height of the label "100" is also clearly measured and the height is found to be about $100\,\mu$m. Since the standard deviation of the ranging accuracy is about $\sigma = 2.7\,\mu$m as shown in Fig. 6(b) and is smaller than the step height of the incuse, the small step height of the incuse can be successfully measured.

In profiling a coin, the reflected light from the surface of the coin is relatively strong and large-amplitude interference signal can be obtained because a coin is made of metal. In order to extend application field of the FMCW optical ranging system, it is necessary to prove that the proposed system is applicable to the object profiling with low surface reflectivity such as a glass and a plastic. Figure 13 is the photograph and the measured profile of a printed circuit board. Plastic-packaged ICs and chip components are clearly profiled, and narrow wiring between ICs and chip components are also profiled. The width of the narrow wiring is about $80\,\mu$m, and then the beam size on the target is deduced to be a few tens μm. We can then conclude that the proposed system is also applicable to inspection in mechanical and electrical assembly process.

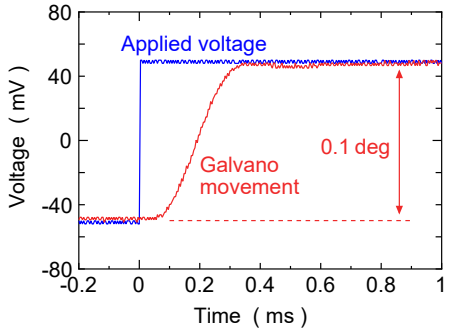

Fig. 14. Step response of the galvano mirror.

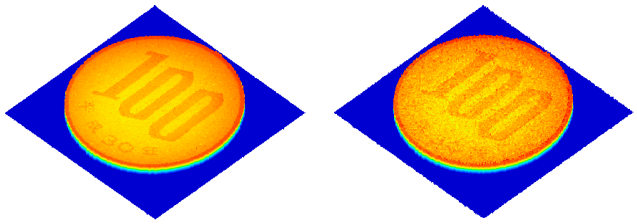

(a) $f_m = 1.3\,\mathrm{kHz}$, 2250 points. (b) $f_m = 1.5\,\mathrm{kHz}$, 2050 points.

Fig. 15. Three-dimensional profiling result of a Japanese 100YEN coin for $f_m = 1.3\,\mathrm{kHz}$ and $f_m = 1.5\,\mathrm{kHz}$.

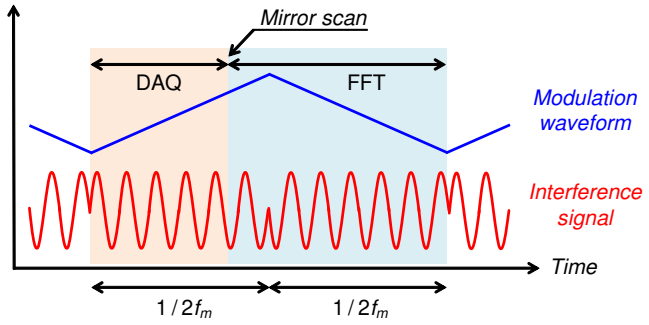

Fig. 16. Modified timings of the data acquisition (DAQ), the galvano mirror scan, and the FFT analysis.

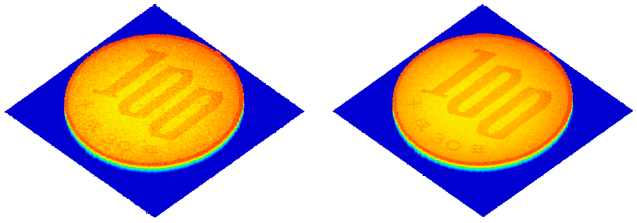

(a) $f_m = 1.5\,\mathrm{kHz}$, 1850 points. (b) $f_m = 1.5\,\mathrm{kHz}$, 1650 points.

Fig. 17. Three-dimensional profiling result of a Japanese 100YEN coin with different number of acquired data for $f_m = 1.5\,\mathrm{kHz}$.

V. Toward Fast Profiling

In the previous experiments, the measurement time for profiling a Japanese 100YEN coin is about 42 sec with 201×201 measurement points since the repetition frequency of the injection current modulation $f_m = 1\,\mathrm{kHz}$ ($201 \times 201 \times 1\,\mathrm{ms}$ = 40.4 sec). The total processing time of the data acquisition and the data transfer from the AD board to the computer is less than $250\,\mu\mathrm{s}$, and then we can profile an object without time delay when the repetition frequency of the injection current modulation $f_m \leq 2\,\mathrm{kHz}$. The other factor of determining the measurement speed is transient property of the galvano mirror.

Figure 14 shown the small signal step response of the galvano mirror. The input voltage is 100 mV which corresponds to the angle change of 0.1 deg. The step response of the galvano mirror is delayed with respect to the input signal, and more than $350\,\mu\mathrm{s}$ is required to stabilize the scan of the galvano mirror ignoring the small ringing around $400 \sim 600\,\mu\mathrm{s}$. This means the maximum repetition frequency of the injection current modulation $f_{m(max)}$ is given as $f_{m(max)} \approx 1/(2 \times 350\,\mu\mathrm{s}) = 1.4\,\mathrm{kHz}$ for the symmetric modulation waveform.

Figure 15 shows the measured profiles of a Japanese 100YEN coin for the repetition frequency of the injection current modulation $f_m = 1.3\,\mathrm{kHz}$ and $f_m = 1.5\,\mathrm{kHz}$, where the modulation current amplitude ΔI for (b) is reduced to $\Delta I = 11\,\mathrm{mA_{p\text{-}p}}$ due to limited operation speed of the k-sampling clock generator, and the number of acquired data is 2250 points and 2050 points for (a) and (b), respectively. The number of points for the FFT analysis is 4096 points. We can get clear profiling result for $f_m = 1.3\,\mathrm{kHz}$, and the profiling result for $f_m = 1.5\,\mathrm{kHz}$ is noisy because the repetition frequency of the injection current modulation $f_m > f_{m(max)} \approx 1.4\,\mathrm{kHz}$. The measurement time for $f_m = 1.3\,\mathrm{kHz}$ is 34 sec.

To improve the profiling quality for high repetition frequency of the injection current modulation f_m, we decrease the number of data to be acquired. The modified timing of the data acquisition (DAQ), the galvano mirror scan and the FFT analysis is shown in Fig. 16. The data acquisition is finished before the turning point of the modulation signal, and then the galvano mirror is immediately scanned to the next position. As a result, enough time is provided for stabilizing the transient response of the galvano mirror. Figure 17 shows the profiling results for $f_m = 1.5\,\mathrm{kHz}$ with the modified timing. The number of acquired data is (a) 1850 points and (b) 1650 points, which are 200 points and 400 points fewer than the number of acquired data of Fig. 15(b). The profiling result becomes clearer by reducing the number of acquired data because the transient behavior of the galvano mirror becomes more stable.

Figure 18 shows the profiling result when the repetition frequency of the injection current modulation $f_m = 1.8\,\mathrm{kHz}$, which is the fastest repetition frequency with clear profiling. The number of acquired data is (a) 1450 points, (b) 1000 points, (c) 800 points, and (d) 600 points. The number of points for the FFT analysis is 4096 points. The modulation current amplitude ΔI is reduced to $\Delta I = 8\,\mathrm{mA_{p\text{-}p}}$ due to limited operation speed of the k-sampling clock generator. It is found that the profiling result becomes clearer with decreasing the number of acquired data, and we can get clear result when the number of acquired data is 600 points as shown in (d). This is because enough time is provided for stabilizing the transient response of the galvano mirror with decreasing the number of acquired data.

However we can see some spike noise in Fig. 18(d). The spike noise can be eliminated by filtering. Figure 19 shows

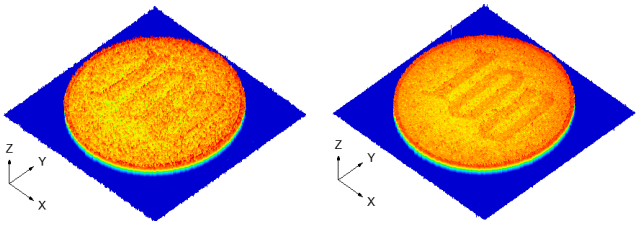

(a) 1450 points. (b) 1000 points.

(c) 800 points. (d) 600 points.

Fig. 18. Three-dimensional profiling results of a Japanese 100YEN coin with different number of acquired data for $f_m = 1.8\,\mathrm{kHz}$.

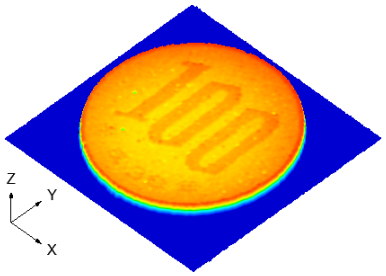

(a) 3×3 moving average filter.

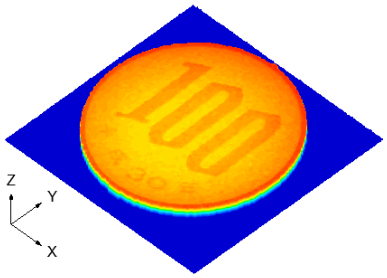

(b) 3×3 median filter.

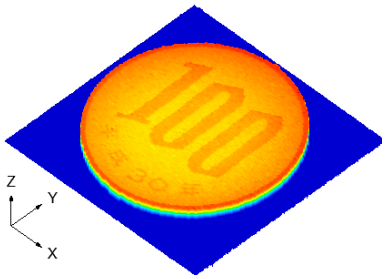

(c) 3-points median filter for x-direction.

Fig. 19. Three-dimensional profiling results of a Japanese 100YEN coin after different types filtering. $f_m = 1.8\,\mathrm{kHz}$ and the number of acquired data is 600 points.

the profiling result after applying (a) a 3×3 moving average filter, (b) a 3×3 median filter, and (c) a 3-points median filter for x-direction. When a 3×3 moving average filter

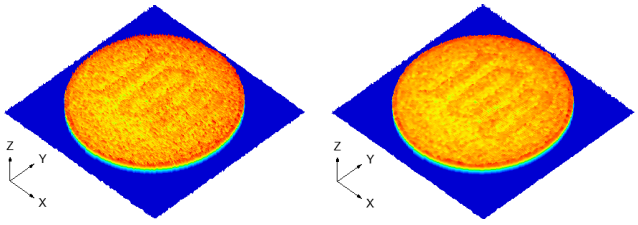

(a) 3-points median filter for x-direction. (b) 3×3 median filter.

Fig. 20. Three-dimensional profiling result of a Japanese 100YEN coin after median filtering to the profiling results shown in Fig. 18(a).

is applied, the profiling result is blurred although the spike noise is eliminated as shown in Fig. 19(a). For median filtering shown in Fig. 19(b) and (c), the spike noise is eliminated and the profiling results are clearer as compared to Fig. 19(a), and 3-points median filtering for x-direction shown in Fig. 19(c) is clearer as compared to 3×3 median filtering shown in Fig. 19(b). Applying a 3-points median filter for y-direction gives similar profiling result with Fig. 19(c). The optimal type of a filter depends on surface profile of an object to be profiled. A moving average filter is a kind of a low pass filter, and then step-like surface profile is smoothed and blurred. Therefore, a moving average filter is effective for profiling smooth surface without step-like profile. A median filter is widely used image filter to eliminate noise without blurring because no averaging is used. Therefore, a median filter is effective for profiling step-like surface such as coins and mechanical workpieces. We tried to apply a 3×3 median filter and a 3-points median filter for x-direction in our study, and which median filter is effective depends on the shape and size of step-like profile.

Although the decreased number of acquired data is very effective to speed-up the measurement time with high quality, the optical frequency sweep range ΔF is also reduced, and the spatial resolution and the ranging accuracy are degraded. The 600 points of acquired data corresponds to the effective optical frequency sweep range $\Delta F \approx 180\,\mathrm{GHz}$, and the FWHM of the beat spectrum and the ranging accuracy can be deduced to be 1.67 mm and about 10 μm from eq. (5) and Fig. 7, respectively. There values are better than the values when the DFB laser is used, and as a results, the profiling result is clearer than the result when the DFB laser is used shown in Fig. 11(a). The measurement time for Fig. 19 is 22.6 sec, which is about 4 times faster than our previous result reported in [16].

Finally we applied a 3-points median filter for x-direction and a 3×3 median filter to the profiling results shown in Fig. 18(a) to confirm effectiveness of median filtering to noisy profiling result, and the results are shown in Fig. 20(a) and (b), respectively. Smoother profiling result is obtained by 3×3 median filtering as compared to 3-points median filtering for x-direction, however the profiling result is still degraded as compared to the profiling results shown in Fig. 19. This means that a median filter is effective to eliminate spike noise and is insufficient for noisy profiling results.

VI. Conclusion

We have developed three-dimensional object profiling system using a highly accurate FMCW optical ranging system.

The laser light is scanned over a target to be profiled, and the spatial distance distribution is measured. High spatial resolution and highly accurate ranging can be realized by using a VCSEL as the frequency-swept laser source because wide optical frequency sweep range is achieved. The experimental spatial resolution defined by the FWHM is $460\,\mu$m and the standard deviation of the measurement error is $\sigma = 2.7\,\mu$m when a VCSEL is used as the frequency-swept laser source. We applied the developed highly accurate FMCW optical ranging system to three-dimensional object profiling, and we have successfully profiled a Japanese 100YEN coin and a printed circuit board. Finally we speed-up the measurement time by increasing the repetition frequency of the injection current modulation and optimizing timing of the data acquisition, the galvano mirror scan and the FFT analysis by taking account of the transient response of the galvano mirror, and the fastest measurement time of 22.6 sec is achieved for 201×201 points measurement points, which is four times faster than our previous results. We also discuss the effect of moving average filtering and median filtering to improve profiling quality, and a median filter is effective to eliminate spike noise.

We can conclude that the developed system is very useful to industrial application such as profiling of mechanical workpieces and inspection in mechanical and electrical assembly process. The developed system is a cost effective system because a low-cost VCSEL is used as the laser source and the optical frequency is swept by the injection current modulation with low repetition frequency. Higher resolution, higher accurate and faster profiling is possible by using a MEMS-VCSEL as the laser source and the system is very useful to medical application such as OCT. However a MEMS-VCSEL is very expensive. We can say that the developed system has enough performance for industrial application with low-cost.

REFERENCES

[1] D. Uttam and B. Culshaw, "Precision time domain reflectometry in optical fiber systems using a frequency modulated continuous wave ranging techniquie," *J. Lightwave Technol.*, vol. LT-3, no. 5, pp. 971–976, October 1985.

[2] G. Economou, R.C. Youngquist, and D.E.N. Davies, "Limitations and noise in interferometric systems using frequency ramped single-mode diode lasers," *J. Lightwave Technol.*, vol. LT-4, no. 11, pp. 1601–1608, November 1986.

[3] H. Barfuss and E. Brinkmeyer, "Modified optical frequency domain reflectometry with high spatial resolution for components of integrated optic systems," *J. Lighwave Technol.*. vol. 7, no. 1, pp. 3–10, January 1989.

[4] W.V. Sorin, D.K. Donald, S. A. Newton, and M. Nazarathy, "Coherent FMCW reflectometry using a temperature tuned Nd:YAG ring laser," *IEEE Photon. Technol. Lett.*, vol. 2, no. 12, pp. 902–904, December 1990.

[5] L.-T. Wang, K. Iiyama, F. Tsukada, N. Yoshida, and K. Hayashi, "Loss measurement in optical waveguide devices by coherent frequency-modulated continuous-wave reflectometry," *Opt. Lett.*, vol. 18, no. 13, pp. 1095–1097, July 1993.

[6] U. Glombitza and E. Brinkmeyer, "Coherent frequency-domain reflectometry for characterization of single-mode integrated-optical waveguides," *J. Lightwave Technol.*, vol. 11, no. 8, pp. 1377–1384, August 1993.

[7] R. Passy, N. Gisin, J.P. von der Weid, and H. H. Gilgen, "Experimental and theoretical investigation of coherent OFDR with semiconductor laser sources," *J. Lightwave Technol.*, vol. 12, no. 9, pp. 1622–1630, Sept. 1994.

[8] B.J. Soller, D.K. Gifford, M.S. Wolfe, and M.E. Froggatt, "High resolution optical frequency domain reflectometry for characterization of components and assemblies," *Opt. Express*, vol. 13, no. 2, pp. 666–674, Jan. 2005.

[9] K. Iiyama, L.-T. Wang, and K. Hayashi, "Linearizing optical frequency sweep of a laser diode for FMCW reflectometry," *J. Lightwave Technol.*, vol. 14, no. 2, pp. 173–178, Feb. 1996.

[10] X. Zhou, K. Iiyama, and K. Hayashi, "Extended-range FMCW Reflectometry Using an Optical Loop with a Frequency Shifter," *IEEE Photon. Technol. Lett.*, vol. 8, no. 2, pp. 248–250, Feb. 1996.

[11] J.P. von der Weid, R. Passy, G. Mussi, and N. Gisin, "On the characterization of optical fiber network components with optical frequency domain reflectometry," *J. Lightwave Technol.*, vol. 15, no. 7, pp. 1131–1141, July 1997.

[12] K. Iiyama, M. Yasuda, and S. Takamiya, "Extended-range high-resolution FMCW reflectometry by means of electronically frequency-multiplied sampling signal generated from auxiliary interferometer," *IEICE Trans. Electon.*, vol. E89-C, no. 6, pp. 823–829, June 2006.

[13] Z. Wang, B. Potsaid, L. Chen, C. Doerr, H.-C. Lee, T. Nielson, V. Jayaraman, A. E. Cable, E. Swanson, and J. G. Fujimoto, "Cubic meter volume optical coherence tomography," *Optica*, vol. 3, Issue 12, pp. 1496–1503, Dec. 2016.

[14] S. Moon and E.S. Choi, "VCSEL-based swept source for low-cost optical coherence tomography," *Biomed. Opt. Express*, vol. 8, no. 2, pp. 1110-1121, Feb. 2017.

[15] K. Iiyama, T. Washizuka, and Y. Kimura, "Three-dimensional object profiling using FMCW optical sensing system," *International Symposium on Optical Memory 2016 (ISOM'16)*, We-K-02, Kyoto, Japan, October 2016.

[16] K. Iiyama, T. Washizuka, and K. Yamaguchi, "Three-dimensional object profiling by FMCW optical ranging system using a VCSEL," *12th Conference on Lasers and Electro-Optics Pacific Rim 2017*, Oral 2-1C-5, Singapore, August 2017.

[17] T. Hariyama, P.A.M. Sandborn, M. Watanabe, and M.C. Wu, "High-accuracy range-sensing system based on FMCW using low-cost VCSEL," *Opt. Express*, vol. 26, no. 7, pp. 9285–9297, April 2018.